Hindawi Publishing Corporation
Journal of Spectroscopy
Volume 2014, Article ID 480102, 7 pages
http://dx.doi.org/10.1155/2014/480102

Research Article

In Situ Dispersive EXAFS in Electrocatalysis: The Investigation of the Local Structure of IrO_x in Chronoamperometric Conditions as a Case Study

Elisabetta Achilli,[1] Alessandro Minguzzi,[2] Ottavio Lugaresi,[2] Cristina Locatelli,[2] Sandra Rondinini,[2] Giorgio Spinolo,[1] and Paolo Ghigna[1]

[1]*Dipartimento di Chimica, Università di Pavia, Via Taramelli 16, 27100 Pavia, Italy*
[2]*Dipartimento di Chimica, Università degli Studi di Milano, Via Golgi 19, 20133 Milano, Italy*

Correspondence should be addressed to Paolo Ghigna; paolo.ghigna@unipv.it

Received 22 October 2014; Revised 16 December 2014; Accepted 18 December 2014; Published 31 December 2014

Academic Editor: Davidson Sajan

An in situ study with dispersive EXAFS (Extended X-Ray Absorption Spectroscopy) at the Ir-L_{III} edge is performed to characterize Electrodeposited Iridium Oxide Films (EIROF) under chronoamperometric conditions. The technique monitors the local chemical environment and electronic structure of iridium during the oxidation of Ir(III) to Ir(IV) with a time resolution of milliseconds. The study is performed in both acidic and basic media. The Fourier transforms of the time-resolved EXAFS signals clearly show that the short-range structure of Ir is similar to that of rutile-type IrO_2 and is maintained during the reaction, thus accounting for the flexibility of the structure of the electrode material in accommodating different oxidation states. From a more general point of view, the work demonstrates the capabilities of in situ experiments based on state-of-the-art dispersive EXAFS in clarifying the mechanistic aspects of electrochemical processes.

1. Introduction

When dealing with the mechanism and the kinetics of heterogeneous catalytic reactions, one of the main challenges is to investigate the processes with sufficient time resolution. The same purpose lies in the investigation of electrocatalytic reactions [1], where the catalysts need to be deposited onto or chemically bound (permanently or just by charge transfer) to a proper conductive support. In order to obtain the maximum number of available active catalytic sites, highly hydrated films and nanostructured materials are usually employed [2]. The observation of changes (in terms of state of charge, local geometric and electronic environment, and structural disorder), linked to the catalytic cycle, does lead to useful information for understanding important mechanistic and kinetic aspects [3, 4]. Thanks to the advent of synchrotron radiation sources it has become possible to exploit the fine structure of the absorption coefficient (XAS: X-Ray Absorption Spectroscopy) in order to get information about both the local geometry and electronic structure [5]. Many XAS experiments have been performed onto electrochemical systems both in transmission and in fluorescence mode. However, one of the main downsides associated with this technique is the time needed for the monochromator to scan over a desired energy range and to settle between movements. A strategy to overcome this limitation is represented by the so-called QUICK-XAS [6] technique, in which the angle of the monochromator is continuously varied. This setup allows acquiring an XAS spectrum in seconds or fractions of seconds. Nevertheless, it should be noted that the time resolution needed to investigate the kinetics and the mechanism of electrocatalytic systems is much higher. The achievement of a finer time resolution and highly focused beams (of dimensions of less than 20 μm) has become possible after the advent of the 3rd generation synchrotron radiation sources. In the setup of a time-resolved-XAS experiment, the standard monochromator is replaced by a polychromator so that the sample is crossed by a polychromatic beam which is

subsequently dispersed onto a detector. This strategy allows recording spectra with a time resolution of milliseconds but only in the transmission mode. In the literature a very small number of time-resolved-XAS studies in the vast field of electrochemistry can be found [7, 8]. Dispersive EXAFS (Extended X-Ray Absorption Fine Structure) experiments are mainly limited by the low energy resolution: the low signal/noise ratio does not allow observing oscillations above $k = 8\,\text{Å}^{-1}$. Thus, reasonable quantitative parameters can be obtained only for the first coordination shells, within ca. 4 Å. In this paper we present a short-range investigation of electrodeposited IrO_x material by means of in situ dispersive EXAFS spectroscopy at the Ir-L_{III} edge aimed at monitoring the local geometrical structure within the second coordination shell of iridium in chronoamperometric conditions. Many reasons lie in the choice of this electrodic material. Iridium oxide is one of the most used anode materials in the electrochemical industrial processes [9–12] such as water electrolysis, cathodic protection, and metal electrowinning, and it is one of the most effective catalysts to promote reactions occurring at advanced photoanodes (most of all, oxidation of water to oxygen). In the literature, Ir catalyst in the water splitting process was proposed to reach the Ir(VI) oxidation state (IrO_3) [13, 14]. In recent works [15, 16], we employed XAS spectroscopy to study the turnover mechanism of Ir catalyst in the water splitting process: Ir was proposed to cycle between the Ir(III) and Ir(V) states. In this context the knowledge of the possible variations in the local chemical structure of Ir with time during the application of different potential steps would be of primary interest; so, in situ time-resolved measurements are processed in order to obtain EXAFS signals for a short-range investigation.

2. Materials and Methods

2.1. Preparation of the Electrodes. The systems consisting of Electrodeposited Iridium Oxide Films (EIROF) are prepared following a modified version of the procedure reported previously [17, 18]. Briefly, 0.0151 g of $IrCl_3{\cdot}3H_2O$ (Alfa Aesar) is dissolved in Milli-Q water (10 mL). After 30 min of stirring, 100 μL of H_2O_2 (30%) is added and the resulting solution is kept under stirring for 30 min. Then, 0.0518 g of oxalic acid is added. The solution is stirred for 10 min. Finally, dried K_2CO_3 is added until pH is about 10.5. The procedure leads to the formation of a yellow solution that turns blue/violet after 3 days at room temperature.

The blue colloid is used as a deposition bath, from which IrO_x is easily deposited onto a conductive support (a carbon disk deposited onto a 175 μm thick polyethylene terephthalate lamina, supplied by Dropsens) at constant current density. We obtained durable and XAS suitable deposits by applying $0.1\,\text{mA cm}^{-2}$ for 600 s, using a Pt plate as the counter electrode.

2.2. Spectroelectrochemical Cell. The cell consists of an empty cylinder made of polytetrafluoroethylene (PTFE, 21 mm diameter, 6 mm thickness, and cavity of 7 mm diameter) that can contain the electrolyte solution (this can be 0.5 M aqueous H_2SO_4 or 1 M aqueous NaOH), a Pt foil counter electrode, and AgCl/Ag in 0.1 M KCl as reference electrode. The reference electrode is separated from the solution by a salt bridge consisting of a glass pipette filled with agar containing 0.2 M aqueous $KClO_4$. One side of the cylinder is closed (the wall being thin enough to not absorb X-ray significantly, i.e., approximately less than 1 mm), while the other one is open to host the working electrode.

The latter electrode is held between the main body of the PTFE cell (through the use of an o-ring) and a second PTFE plate that also includes a hole for the X-rays beam.

2.3. Dispersive XAS Measurements. Dispersive XAS data were collected at ID24 beamline [19, 20] at the European Synchrotron Radiation Facility, ESRF, Grenoble (the ring energy is 6.0 GeV and the current 150–200 mA). The X-ray source consisted of two ondulators whose gaps were adjusted to tune constant counts of the first harmonic for energies around the Ir-L_{III} edge along the spectra. The beam was focused horizontally by a curved polychromator (Si 111) crystal in Bragg geometry and vertically with a bent Si mirror at a glancing angle of 2.5 mrad with respect to the direct beam. The beam size at the sample was 8 mm FWHM horizontally and 80 mm FWHM vertically in order to decrease the photon density in order to preserve the samples.

Spectra were recorded in transmission mode using a FreLonCCD camera detector [21]. The energy calibration was made by measuring the absorption spectrum of a Pt foil (Pt-L_{III}: 11564 eV; Ir-L_{III}: 11215 eV).

Sequences of spectra were acquired while applying different chronoamperometry protocols. Series of 10000 and 20000 spectra were acquired in 116 and 232 seconds, respectively (each single spectrum is registered every 0.0116 s). Averages were calculated every 10 spectra in order to obtain a better signal-to-noise ratio: this gives a final time resolution equal to 0.116 s. The experiment was repeated with two different kinds of electrolyte (0.5 M aqueous H_2SO_4 and 1 M aqueous NaOH) with the application of different potential steps (both in oxidation and in reduction). Each step was carried out after a prolonged (≥180 s) preconditioning at the initial condition (starting potential). The potential step was triggered by the spectra acquisition system through the trigger option of the potentiostat (a CH Instrument 630D). All measurements were carried out at room temperature.

2.4. Data Processing and Analysis. The main stages of data analysis were (i) the extraction of the EXAFS signals with the pertinent Fourier transforms (FTs) and (ii) the fit of the structural model. EXAFS data extraction, performed with the PRESTOPRONTO software (in preparation), started from the evaluation a *pre-edge* and a *post-edge* baseline function (Figure 1) that were then applied to the row signal. The first function is associated with additional excitations of the photoabsorber or with possible excitations of any other element present ($\mu_n x$) and was modeled with a straight line obtained by interpolating the *pre-edge* data and then extrapolated to the post-edge signal. The latter function represents the absorption profile due to an isolated photoabsorber (hereafter

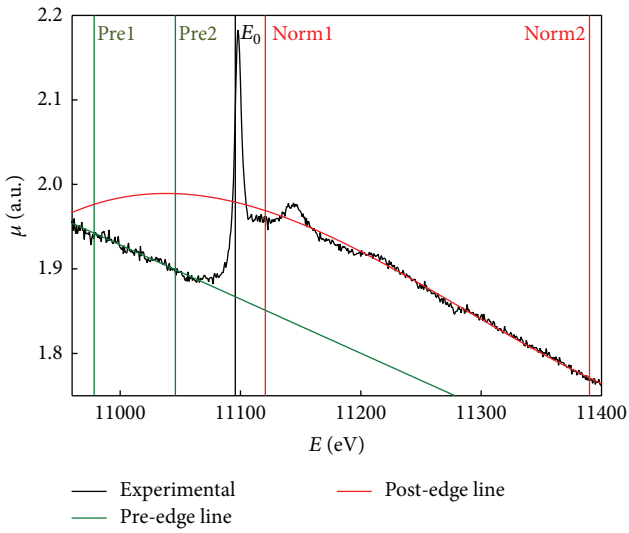

Figure 1: EXAFS signal extraction: the experimental XAS spectrum is the blue line, the *pre-edge* function is represented as a green line, and the *post-edge* function is represented as a red line.

denoted by $\mu_0(E)$) and was modeled with a 3rd order spline using the first inflection point as E_0. The interval for the pre-edge fitting and the interval for the post-edge fittings were the same for an entire sequence of measurements but only some representative spectra were chosen for the subsequent EXAFS analysis and fitting.

The extracted EXAFS signal was then fitted to an appropriate structural model with the EXCURVE code [22]. The calculation of the atomic scattering parameters (phases and amplitudes) was based on the muffin-tin approximation, in the framework of the Hedin-Lundquist and Von Bart approximations for the exchange and ground state potentials, respectively [22]. This includes the effects of losses due to the electron inelastic scattering. The fittings were made in the k space, using a k^2 weighting scheme and full multiple scattering calculation within the assumed clusters. The number of EXAFS independent points, given by $2(\Delta k \times \Delta r)/\pi$, is ca. 6.

As goodness of fit (GOF) we used the F-factor:

$$F = 100 \sum_{i}^{N} \frac{\left[\chi_{i,\text{exp}} - \chi_{i,\text{calc}}\right]^2}{\sigma_i}. \quad (1)$$

3. Results and Discussion

After visual inspection of the signal after the extraction step, full EXAFS data processing was performed for only some spectra selected from the entire data set, with the aim of gaining structural information concerning initial and final stages of the reactive process and a few intermediate advancement degrees. Figure 2 shows the response to a potential step from 0.2 to 1.05 V versus RHE, that is, corresponding to the oxidation of Ir(III) to Ir(IV), as reported in our previous papers [15, 16]. The measurements have been acquired using acidic medium as electrolyte. The sequence of EXAFS spectra reported in Figure 2 with the corresponding FTs has been recorded at time intervals of ca. 6 s within the first 40 s: at that time, the oxidation process has surely reached its end, as shown by the fact that simultaneously the chronoamperometric signal shows zero current. EXAFS oscillations are visible up to $k = 8\,\text{Å}^{-1}$ thus allowing us to characterize the first and the second coordination shells.

The similarity that can be observed between the signals at different times clearly demonstrates that the local structure (at least within the first two shells) is maintained during the reaction. A comparison with the standard spectrum (black trace) also demonstrates that the local structure of Ir is very similar to that found in rutile-type IrO_2. The FT's peak at ca. 1.5 Å, in particular, corresponds to the 6 O neighbors in the rutile structure. The peaks between 3.4 and 3.8 Å are mainly due to Ir and O atoms that are the next nearest neighbors (NNN) around Ir of IrO_2. This is by itself a quite remarkable result, if attention is paid to the fact that at the beginning of the reaction Ir is present as Ir(III), and nicely demonstrates the flexibility of the EIROF matrix in accommodating different oxidation states.

Similar considerations apply to the spectra acquired in basic medium (Figure 3). Again, EXAFS and FT spectra do not show considerable variations during the course of the reaction, as the local structure remains almost the same during the entire time period of data acquisition.

Interestingly, the comparison of the FTs of the spectra acquired in acidic and basic media (Figure 4) highlights a difference in the first coordination peaks. The red line, showing the signal acquired in acidic medium, shows an additional shoulder towards lower distance values. The result clearly marks the presence of a smaller Ir–O bond distance. By comparison, the blue line, pertinent to the measurements in basic medium, is characterized by a clearly narrower first-coordination-shell peak with a maximum at a larger distance value: this feature can be explained by the presence of six equal Ir–O bond distances.

The inference can be made more precise and quantified by fitting the EXAFS with a structural model essentially based on rutile-type IrO_2 (as suggested by the experimental evidence) and discussing the parameters so retrieved. According to crystallographic information [23–25], the radii of the shells are those reported in Tables 1 and 2 under the headings (r^*). As a technical detail, we remark the tetragonal symmetry of the basic structural model, so that precise octahedral coordination of oxygen around Ir, when requested, can be simulated using an additional constraint, which sets to equal values two distances that are not constrained by tetragonal symmetry to be equal.

As far as the acidic medium is concerned, the fit model consists of iridium in a compressed octahedral site, with two axial oxygen atoms placed at a shorter distance than the equatorial ones (see below for further details). The third shell consists of two iridium atoms and the fourth one consists of four oxygen atoms. Full multiple scattering calculations making use of the exact curved wave theory were performed to fit the spectra. The best-fit results are shown in Figure 5 as a red line whereas the black line illustrates the experimental data.

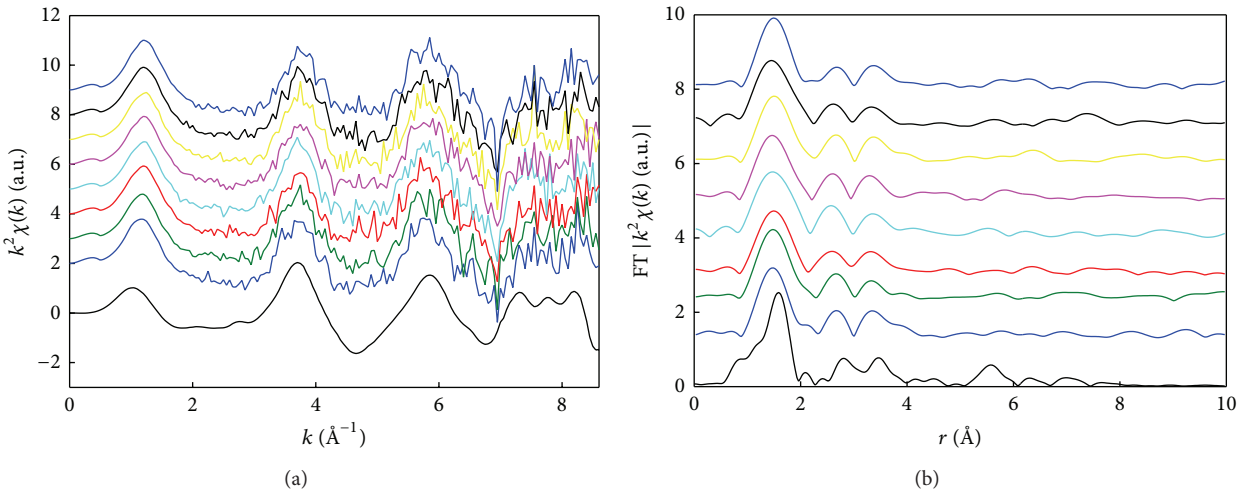

Figure 2: EXAFS (a) and FT (b) spectra of a sequence recorded within the first 40 seconds illustrated from the bottom to the top, separated by a time interval of ca. 6 seconds. The IrO_2 standard EXAFS and FT signals are represented as black lines. Measurements were carried out in acidic medium for the potential step 0.2–1.05 V.

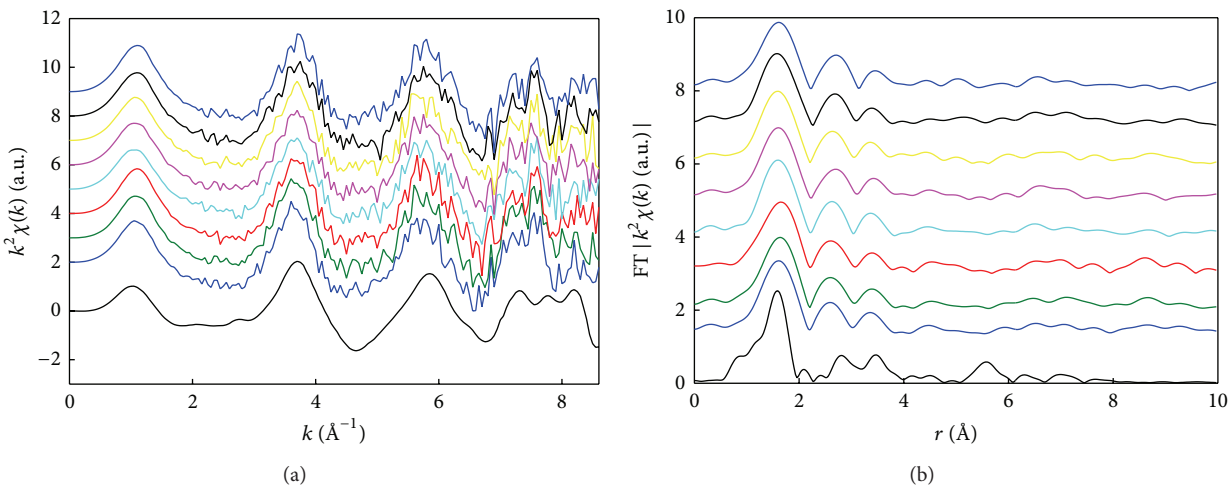

Figure 3: EXAFS (a) and FT (b) spectra of a sequence recorded within the first 40 seconds illustrated from the bottom to the top, separated by a time interval of ca. 6 seconds. The IrO_2 standard EXAFS and FT signals are represented as black lines. Measurements were carried out in basic medium for the potential step 0.2–0.9 V.

Table 1 shows the structural parameters obtained by the fitting procedure for different reaction times (i.e., after 0.23, 5.2, 10.0, and 34.8 s) in acidic medium. The radii of the second and the third shell (and the coordination numbers of all the shells, as well) were kept constant at the crystallographic values in order to avoid correlation due to too large ratio of number of parameters to amount of data (as mentioned before, the time-resolved technique has prevented us from achieving a larger energy resolution and thus a large value of the EXAFS independent data points); however, it should be noted that the addition of these further shells is needed to obtain a good fit. In all cases, the F values are between ca. 25 and ca. 30%. These figures indicate a good fit, given also the unavoidable level of noise that affects the spectra presented here, collected in 116 μs.

According to the previous comments, the spectra acquired in alkaline medium were fitted with a model consisting of a first coordination shell of six oxygen atoms in an exactly octahedral arrangement (Figure 5 and Table 2).

The fitting parameters so retrieved are shown in Table 2. First of all, we note a negative trend with time of the first Ir–O distances, as expected for a process going from Ir(III) to Ir(IV). The distances for the sample at the last time are markedly close to the mean value of the crystallographic distances for IrO_2. Then, at all times the distances are significantly larger than those obtained in acidic medium. Finally, in this case the goodness of fit values (F) are smaller than 30%, a result that is a direct support to the inference of perfect octahedral arrangements of oxygen in the first coordination shell. A reasonable explanation to this structural difference

Table 1: EXAFS fitting parameters obtained for spectra acquired at 0.23, 5.2, 10.0, and 34.8 s in acidic medium; r: distances; σ^2: distance variances; r^*: crystallographic values; the coordination numbers N have been kept constant to their crystallographic values.

			0.23 s						5.2 s		
Shell	N	Atom	r (Å)	σ^2 (Å^2)	r (Å)*	Shell	N	Atom	r (Å)	σ^2 (Å^2)	r (Å)*
1	2	O	1.64 (7)	$3\ (2) * 10^{-2}$	1.943	1	2	O	1.65 (9)	$3\ (3) * 10^{-2}$	1.943
2	4	O	1.88 (2)	$0\ (1) * 10^{-3}$	1.980	2	4	O	1.89 (3)	$0\ (2) * 10^{-3}$	1.980
3	2	Ir	3.110	$3\ (9) * 10^{-2}$	3.110	3	2	Ir	3.110	$2\ (9) * 10^{-2}$	3.110
4	4	O	3.406	$1\ (2) * 10^{-2}$	3.406	4	4	O	3.406	$1\ (2) * 10^{-2}$	3.406
			F = 27.8%						F = 32.4%		
			10.0 s						34.8 s		
Shell	N	Atom	r (Å)	σ^2 (Å^2)	r (Å)*	Shell	N	Atom	r (Å)	σ^2 (Å^2)	r (Å)*
1	2	O	1.70 (9)	$4\ (3) * 10^{-2}$	1.943	1	2	O	1.70 (9)	$4\ (3) * 10^{-2}$	1.943
2	4	O	1.91 (2)	$0\ (2) * 10^{-3}$	1.980	2	4	O	1.90 (2)	$1\ (2) * 10^{-3}$	1.980
3	2	Ir	3.110	$0\ (1) * 10^{-2}$	3.110	3	2	Ir	3.110	$1\ (2) * 10^{-2}$	3.110
4	4	O	3.406	$1\ (2) * 10^{-2}$	3.406	4	4	O	3.406	$1\ (3) * 10^{-2}$	3.406
			F = 24.3%						F = 26.0%		

Table 2: EXAFS fitting parameters obtained for spectra acquired at 0.23, 5.2, 10.0, and 34.8 s in alkaline medium; r: distances; σ^2: distance variances; r^*: crystallographic values; the coordination numbers N have been kept constant to their crystallographic values.

			0.23 s						5.2 s		
Shell	N	Atom	r (Å)	s^2 (Å^2)	r (Å)*	Shell	N	Atom	r (Å)	s^2 (Å^2)	r (Å)*
1	2	O	2.00 (2)	$5\ (2) * 10^{-3}$	1.943	1	2	O	1.98 (2)	$5\ (2) * 10^{-3}$	1.943
2	4	O	2.00 (2)	$5\ (2) * 10^{-3}$	1.980	2	4	O	1.98 (2)	$5\ (2) * 10^{-3}$	1.980
3	2	Ir	3.110	$1\ (9) * 10^{-3}$	3.110	3	2	Ir	3.110	$1\ (8) * 10^{-3}$	3.110
4	4	O	3.406	$1\ (2) * 10^{-2}$	3.406	4	4	O	3.406	$1\ (3) * 10^{-2}$	3.406
			F = 25.9%						F = 26.3%		
			10.0 s						34.8 s		
Shell	N	Atom	r (Å)	s^2 (Å^2)	r (Å)*	Shell	N	Atom	r (Å)	s^2 (Å^2)	r (Å)*
1	2	O	1.97 (2)	$5\ (2) * 10^{-3}$	1.943	1	2	O	1.96 (2)	$3\ (2) * 10^{-3}$	1.943
2	4	O	1.97 (2)	$5\ (2) * 10^{-3}$	1.980	2	4	O	1.96 (2)	$3\ (2) * 10^{-3}$	1.980
3	2	Ir	3.110	$0\ (9) * 10^{-3}$	3.110	3	2	Ir	3.110	$0\ (8) * 10^{-3}$	3.110
4	4	O	3.406	$1\ (2) * 10^{-2}$	3.406	4	4	O	3.406	$0\ (2) * 10^{-2}$	3.406
			F = 26.7%						F = 23.5%		

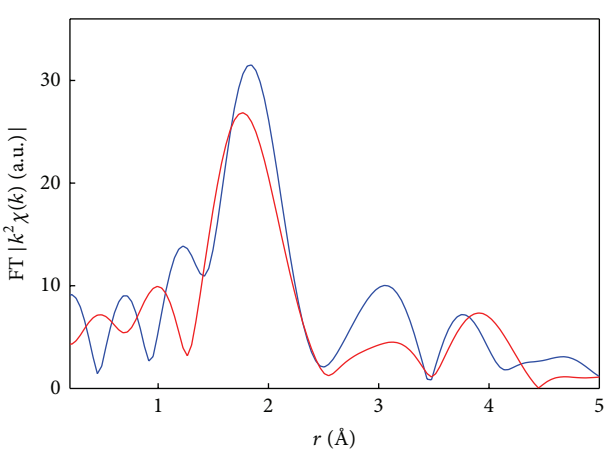

Figure 4: Comparison of the first peak of the Fourier transforms recorded in acidic medium (red line) and in alkaline medium (blue line).

between acidic and basic medium lies in the protonation of the two axial oxygen atoms in acidic medium.

4. Conclusions

Dispersive EXAFS has been demonstrated to be a powerful tool for exploring the local chemical environment of materials with a subsecond time resolution. This paper illustrates, as a case study, an in situ application of the technique, at the Ir-L_{III} edge, to assess the chemical environment of Ir in Electrodeposited Iridium Oxide Films (EIROF) while applying chronoamperometric conditions corresponding to the oxidation of Ir(III) to Ir(IV).

EXAFS shows that the local structure around Ir remains constant during the oxidation process and is quite similar to that of rutile-type IrO_2, a nice proof of the high flexibility of the EIROF matrix that is able to accommodate both oxidation states of Ir.

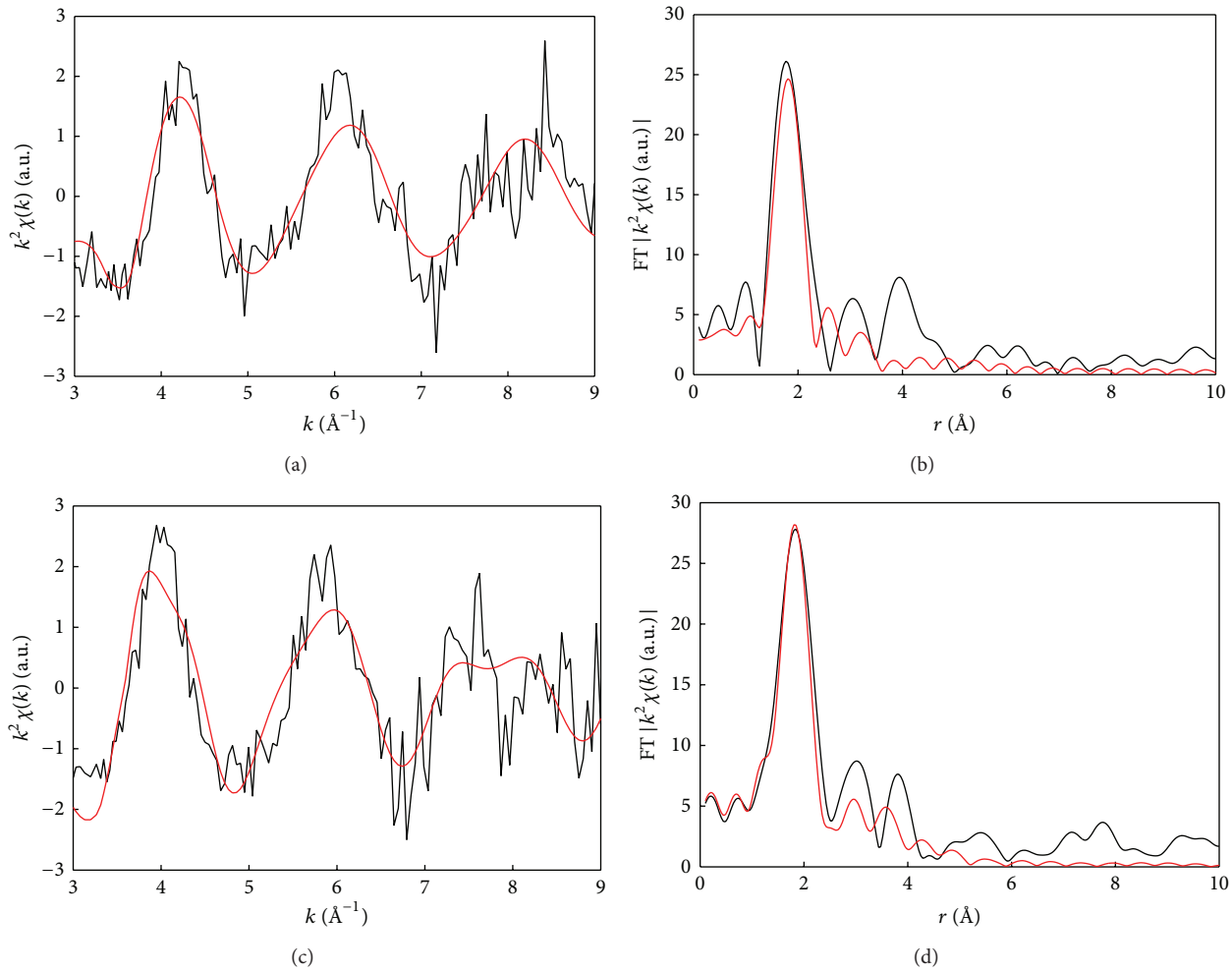

Figure 5: Fitting of EXAFS (a) and relative FT (b) spectra in acidic and (c and d) basic medium. The experiment is the black line whereas the theory according to the structural model of Table 2 is represented as a red line.

The technique is also capable of highlighting finer structural details, such as a difference in dimension and distortion of the first coordination shell. Experiments in acidic medium show that the coordination octahedra are remarkably distorted, with a shorter Ir–O bond for the axial oxygen. Experiments in basic medium indicate generally longer distances and do not show distortion of the octahedral arrangement.

It is suggested that the result can be explained by protonation of the axial oxygen atoms in acidic medium.

Conflict of Interests

The authors declare that there is no conflict of interests regarding the publication of this paper.

Acknowledgments

ESRF is acknowledged for providing beamtime (Exp. CH-4090). The authors would also like to thank the beamline staff and in particular Dr. Giovanni Agostini for his help during the data collection.

References

[1] Y.-F. Huang, D.-Y. Wu, A. Wang et al., "Bridging the gap between electrochemical and organometallic activation: benzyl chloride reduction at silver cathodes," *Journal of the American Chemical Society*, vol. 132, no. 48, pp. 17199–17210, 2010.

[2] M. A. Méndez, L. Alibabei, J. J. Concepcion, and T. J. Meyer, "Electrocatalysis on oxide-stabilized, high-surface area carbon electrodes," *ACS Catalysis*, vol. 3, pp. 1850–1854, 2013.

[3] A. Minguzzi, O. Lugaresi, C. Locatelli et al., "Fixed energy X-ray absorption voltammetry," *Analytical Chemistry*, vol. 85, no. 15, pp. 7009–7013, 2013.

[4] A. Minguzzi, O. Lugaresi, E. Achilli et al., "Observing the oxidation state turnover in heterogeneous iridium-based water oxidation catalysts," *Chemical Science*, vol. 5, no. 9, pp. 3591–3597, 2014.

[5] B. K. Teo, *EXAFS: Basic Principles and Data Analysis*, Springer, 1986.

[6] C. Prestipino, O. Mathon, R. Hino, A. Beteva, and S. Pascarelli, "Quick-EXAFS implementation on the general purpose EXAFS beamline at ESRF," *Journal of Synchrotron Radiation*, vol. 18, no. 2, pp. 176–182, 2011.

[7] R. O'Malley, A. Vollmer, J. R. I. Lee et al., "Time-resolved studies of diffusion via energy dispersive X-ray absorption spectroscopy," *Electrochemistry Communications*, vol. 5, no. 1, pp. 1–5, 2003.

[8] A. Rose, O. South, I. Harvery, S. Diaz-Moreno, J. R. Owen, and A. E. Russell, "*In situ* time resolved studies of hydride and deuteride formation in Pd/C electrodes via energy dispersive X-ray absorption spectroscopy," *Physical Chemistry Chemical Physics*, vol. 7, pp. 366–372, 2005.

[9] A. Minguzzi, F.-R. F. Fan, A. Vertova, S. Rondinini, and A. J. Bard, "Dynamic potential-pH diagrams application to electrocatalysts for water oxidation," *Chemical Science*, vol. 3, no. 1, pp. 217–229, 2012.

[10] M. Carmo, D. L. Fritz, J. Mergel, and D. Stolten, "A comprehensive review on PEM water electrolysis," *International Journal of Hydrogen Energy*, vol. 38, no. 12, pp. 4901–4934, 2013.

[11] J.-P. G. de Mussy, J. V. Macpherson, and J.-L. Delplancke, "Characterisation and behaviour of Ti/TiO_2/noble metal anodes," *Electrochimica Acta*, vol. 48, no. 9, pp. 1131–1141, 2003.

[12] P. Pedeferri, "Cathodic protection and cathodic prevention," *Construction and Building Materials*, vol. 10, no. 5, pp. 391–402, 1996.

[13] S. Fierro, A. Kapałka, and C. Comninellis, "Electrochemical comparison between IrO_2 prepared by thermal treatment of iridium metal and IrO_2 prepared by thermal decomposition of H_2IrCl_6 solution," *Electrochemistry Communications*, vol. 12, no. 1, pp. 172–174, 2010.

[14] T. Nakagawa, C. A. Beasley, and R. W. Murray, "Efficient electro-oxidation of water near its reversible potential by a mesoporous IrO_x nanoparticle film," *The Journal of Physical Chemistry C*, vol. 113, no. 30, pp. 12958–12961, 2009.

[15] A. Minguzzi, O. Lugaresi, C. Locatelli et al., "Fixed energy X-ray absorption voltammetry," *Analytical Chemistry*, vol. 85, no. 15, pp. 7009–7013, 2013.

[16] A. Minguzzi, O. Lugaresi, E. Achilli et al., "Observing the oxidation state turnover in heterogeneous iridium-based water oxidation catalysts," *Chemical Science*, vol. 5, no. 9, pp. 3591–3597, 2014.

[17] K. Yamanaka, "Anodically electrodeposited iridium oxide-films (Aeirof) from alkaline-solutions for electrochromic display devices," *Japanese Journal of Applied Physics*, vol. 28, no. 4, pp. 632–637, 1989.

[18] M. A. Petit and V. Plichon, "Anodic electrodeposition of iridium oxide films," *Journal of Electroanalytical Chemistry*, vol. 444, no. 2, pp. 247–252, 1998.

[19] S. Pascarelli, O. Mathon, M. Munõz, T. Mairs, and J. Susini, "Energy-dispersive absorption spectroscopy for hard-X-ray micro-XAS applications," *Journal of Synchrotron Radiation*, vol. 13, no. 5, pp. 351–358, 2006.

[20] S. Pascarelli and O. Mathon, "Advances in high brilliance energy dispersive X-ray absorption spectroscopy," *Physical Chemistry Chemical Physics*, vol. 12, no. 21, pp. 5535–5546, 2010.

[21] J.-C. Labiche, O. Mathon, S. Pascarelli et al., "Invited article: the fast readout low noise camera as a versatile x-ray detector for time resolved dispersive extended x-ray absorption fine structure and diffraction studies of dynamic problems in materials science, chemistry, and catalysis," *Review of Scientific Instruments*, vol. 78, no. 9, Article ID 091301, 2007.

[22] N. Binsted and S. S. Hasnain, "State-of-the-art analysis of whole X-ray absorption spectra," *Journal of Synchrotron Radiation*, vol. 3, pp. 185–196, 1996.

[23] S. Gražulis, A. Daškevič, A. Merkys et al., "Crystallography Open Database (COD): an open-access collection of crystal structures and platform for world-wide collaboration," *Nucleic Acids Research*, vol. 40, no. 1, pp. D420–D427, 2012.

[24] S. Graulis, D. Chateigner, R. T. Downs et al., "Crystallography open database—an open-access collection of crystal structures," *Journal of Applied Crystallography*, vol. 42, no. 4, pp. 726–729, 2009.

[25] R. T. Downs and M. Hall-Wallace, "The American Mineralogist crystal structure database," *The American Mineralogist*, vol. 88, no. 1, pp. 247–250, 2003.